photonics

MDPI

Article

An Efficient Method for Wavefront Aberration Correction Based on the RUN Optimizer

Huizhen Yang [1], Xiangdong Zang [2], Peng Chen [1], Xingliu Hu [1], Yongqiang Miao [2], Zhaojun Yan [3,*] and Zhiguang Zhang [2]

[1] Engineering School of Networks & Telecommunications, Jinling Institute of Technology, Nanjing 211169, China; yanghz@jit.edu.cn (H.Y.); chenpeng375@jit.edu.cn (P.C.); jimmy080@jit.edu.cn (X.H.)
[2] School of Electronic Engineering, Jiangsu Ocean University, Lianyungang 222005, China; zangxiangdong@jou.edu.cn (X.Z.); miaoyongqiang@jou.edu.cn (Y.M.); zhangzhiguang10@mails.ucas.ac.cn (Z.Z.)
[3] The Astronomical Optical Instrument Group, Shanghai Astronomical Observatory, Chinese Academy of Sciences, Shanghai 200030, China
* zhaojunyan@shao.ac.cn

Abstract: The correction of wavefront aberrations in wavefront sensorless (WFS-less) adaptive optical (AO) systems requires control algorithms that can ensure rapid convergence while maintaining effective correction capabilities. This paper proposes a novel control algorithm based on the RUNge Kutta optimizer (RUN) for WFS-less AO systems that enables the quick and efficient correction of small aberrations, as well as larger aberrations. To evaluate the convergence speed and correction capabilities of a WFS-less AO system based on the RUN control algorithm, we constructed a simulated AO system and an experimental setup with a 97-element deformable mirror (DM), respectively. Additionally, the results obtained with the Particle Swarm Optimization (PSO) algorithm, Differential Evolution Algorithm (DEA), and Genetic Algorithm (GA) are also provided for comparison and analysis. Both the simulated and experimental results consistently demonstrated that our proposed method outperformed several competing algorithms in terms of correction performance and convergence speed. Furthermore, the experimental results further validate the effectiveness of our control algorithm in scenarios involving significant aberrations.

Keywords: adaptive optics; control algorithm; RUNge Kutta optimizer; deformable mirror; wavefront correction

check for updates

Citation: Yang, H.; Zang, X.; Chen, P.; Hu, X.; Miao, Y.; Yan, Z.; Zhang, Z. An Efficient Method for Wavefront Aberration Correction Based on the RUN Optimizer. *Photonics* **2024**, *11*, 29. https://doi.org/10.3390/photonics11010029

Received: 15 November 2023
Revised: 20 December 2023
Accepted: 27 December 2023
Published: 28 December 2023

Copyright: © 2023 by the authors. Licensee MDPI, Basel, Switzerland. This article is an open access article distributed under the terms and conditions of the Creative Commons Attribution (CC BY) license (https://creativecommons.org/licenses/by/4.0/).

1. Introduction

The adaptive optics (AO) technology is an indispensable tool for correcting static or dynamic aberrations caused by light passing through a random medium or an imperfect imaging system [1–3]. AO systems can be classified into conventional AO systems and wavefront sensorless (WFS-less) AO systems. WFS-less AO systems have been successfully applied in various applications, including free-space optical communication [4,5], extended object imaging [6,7], and multi-photon microscopy for biological imaging [8]. The simplicity and ease of implementation of the system structure make WFS-less AO systems suitable for environments where traditional AO systems are not feasible. Generally, the performance of WFS-less AO systems heavily relies on the control algorithm that is employed.

The existing control algorithms for WFS-less AO systems can be broadly classified into the following categories: metaheuristic methods based on population optimization, such as the Genetic Algorithm (GA) [9,10], Particle Swarm Optimization (PSO) [11,12], Differential Evolution Algorithm (DEA) [13], etc.; gradient descent methods based on mathematical principles, such as the Stochastic Parallel Gradient Descent (SPGD) algorithm [14] and its various variants [15–17]; model-based approaches grounded in physical principles and their improved algorithms [18–21]. These three types of methods have been employed

in the control of adaptive optical systems, with each possessing its own strengths and weaknesses. For instance, metaheuristic algorithms exhibit relatively slow convergence speed but possess good global convergence capabilities. On the other hand, the SPGD method demonstrates relatively fast convergence speed but lacks global optimization ability. Model-based algorithms converge at the fastest rate but require extensive preprocessing. Additionally, the advancement of artificial intelligence has led to the implementation of deep learning and artificial neural network technology for controlling AO systems [22–24]. Machine learning algorithms have good real-time performance, but they require a large amount of training data, and the training samples are often different from the data in actual applications.

The RUNge Kutta optimizer (RUN), which was proposed by Ahmadianfar et al. in 2021 [25], is a metaphor-free, swarm-based metaheuristic algorithm that utilizes the fourth-order Runge-Kutta (RK) [26,27] mathematical approach to calculate gradients. It employs this method as a global search strategy for effectively exploring the target region within the search space. The RUN optimization algorithm has demonstrated its capability in handling various optimization problems and has been successfully applied in engineering domains such as thermodynamics [28] and power engineering [29].

The application of the RUN optimizer to the control of adaptive optical systems is proposed in this paper, in addition to a corresponding control algorithm. Additionally, a simulated AO system and an experimental setup were constructed with a 97-element DM for the point source. The convergence speed and correction capabilities of a WFS-less AO system based on the RUN control algorithm were investigated through a simulation analysis and experimental verification. For comparison, we also provide the aforementioned results obtained with PSO, DEA, and GA.

2. Principles of the AO Control Method Based on the RUN Optimizer

The primary search mechanism of the RUN-based AO system utilizes the fourth-order RK method, which allows for both global and local searches [25]. Let $y(x)$ be the objective function, where x is an M-dimensional particle. The M-dimensional particle represents the position of the particle, which corresponds to the driving voltage vector of the wavefront corrector in AO systems. The fourth-order RK formula is derived from a weighted average of four coefficients and is computed as follows:

$$y(x + \Delta x) = y(x) + \frac{1}{6}(k_1 + 2k_2 + 2k_3 + k_4)\Delta x \tag{1}$$

where the four coefficients k_1, k_2, k_3, and k_4 are:

$$k_1 = y'(x) = f(x) \tag{2}$$

$$k_2 = f(x + \frac{\Delta x}{2}, y + k_1\frac{\Delta x}{2}) \tag{3}$$

$$k_3 = f(x + \frac{\Delta x}{2}, y + k_2\frac{\Delta x}{2}) \tag{4}$$

$$k_4 = f(x + \Delta x, y + k_3\Delta x) \tag{5}$$

The driving voltage of the wavefront corrector serves as the control signal, while the particle position represents the voltage of the corrector. During the iteration process of the algorithm, population particles are explored and exploited within the search space in order to achieve optimal results. The RUN-based AO control method mainly consists of an initialization stage, a position update stage, and a correction stage. To ensure the solution quality, an enhanced solution quality (ESQ) component [25] is utilized in the position update stage to effectively prevent getting trapped in local extrema during each iteration.

The initialization stage consists of initializing the particle position and applying the initial position to the wavefront corrector. Image information is acquired from a charge-coupled device (CCD) camera and then fed into the control module. The objective

function of the optimization algorithm is determined based on a performance metric that characterizes the extent of the wavefront aberration. In the position update stage, the fourth-order RK method is employed as the primary mechanism for exploration and exploitation, as it enables effective global and local searches. This stage completes the position update of each particle in the population and makes necessary adjustments. During the correction stage, the current global optimal solution is digitally converted, amplified, and applied to the wavefront corrector to correct the residual wavefront, thereby completing one iteration. The flow of the AO control algorithm based on RUN is shown in Figure 1.

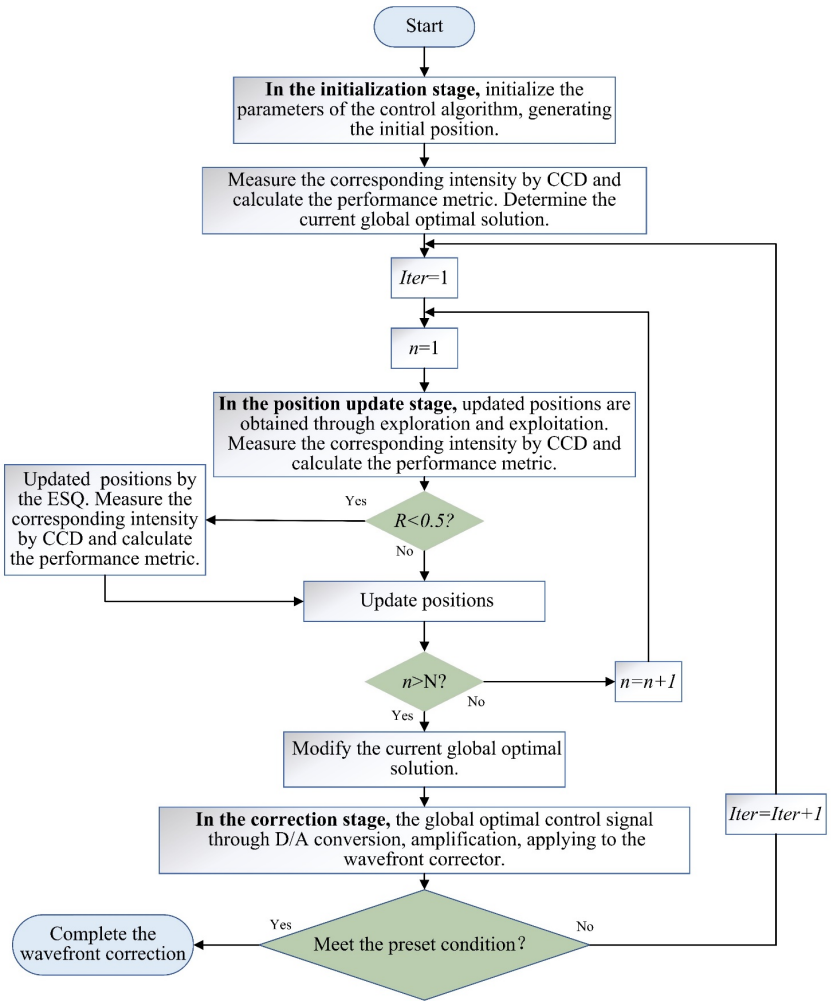


Figure 1. A flowchart of the AO control algorithm based on RUN.

3. Analysis of Simulations and Results

3.1. The Wavefront Sensorless AO System

The WFS-less AO system, as shown in Figure 2, was based on the RUN optimizer. In this system, a 97-element DM was utilized as the wavefront corrector, and a CCD camera served as the image sensor. The system was mainly composed of a DM, a CCD, a lens, a control module, an image acquisition card, a digital-to-analog converter, and a high-voltage amplifier. When light passed through the medium, the incident light wave underwent wavefront distortion, and the distorted incident light was reflected through the deformable mirror and then reached the CCD camera for imaging through the lens. The AO system control method based on RUN calculated the control signal of the DM using the imaging signal acquired by the image acquisition card. The digital-to-analog converter converted the control signal into an analog signal, and then the high-voltage amplifier amplified the control signal and applied it to the deformable mirror to complete a closed-loop correction.

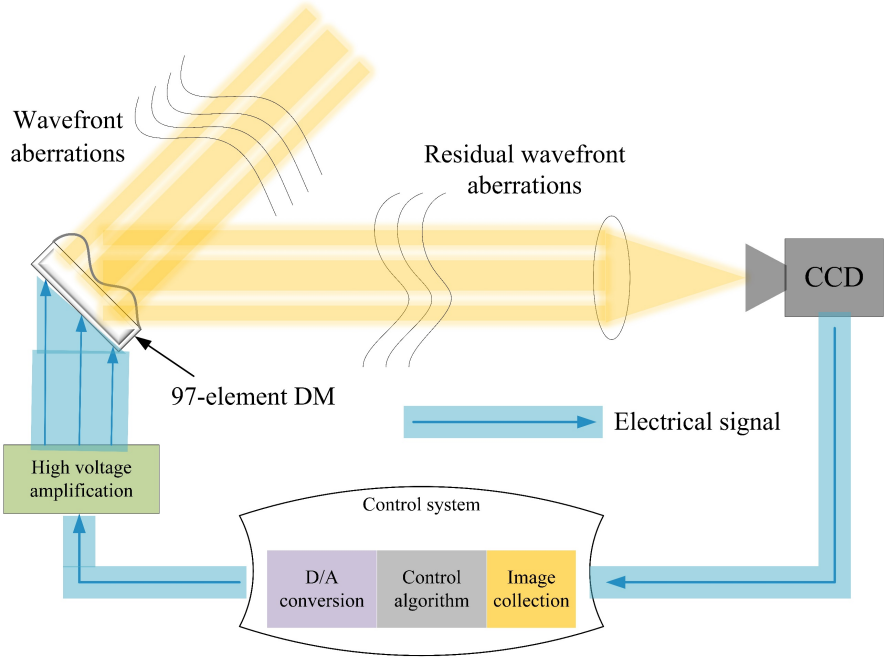


Figure 2. A schematic diagram of the wavefront correction system.

The arrangement of the actuators for the 97-element DM is shown in Figure 3; they were organized in a square pattern. Each actuator is represented by a red circle, while the effective aperture of the DM is depicted by a blue circle with a diameter of 22.5 mm. Based on the parameters of the simulation system for the point source imaging, the ideal MR was 4.62 pixels.

Multi-frame phase screens were generated using Roddier's method [30] as wavefront aberrations to be corrected. These phase screens complied with the Kolmogorov power spectrum model, and no correlation was exhibited between them. Zernike polynomials ranging from mode 3 to 104 (excluding the tilt term) were employed to construct these phase screens. The turbulence level was quantified by D/r_0, where D is the telescope diameter and r_0 denotes the atmospheric coherence length [31].

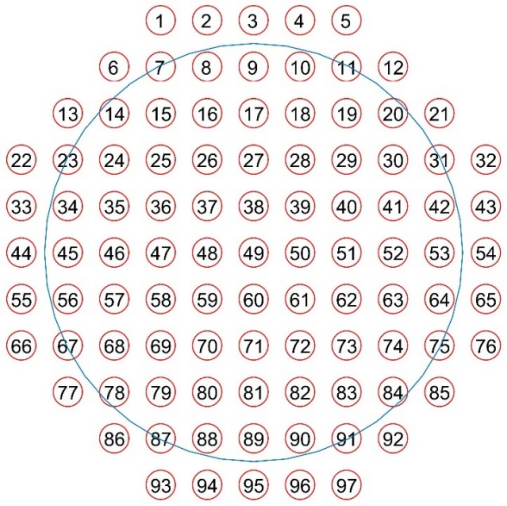


Figure 3. The spatial distribution of the actuators of a 97-element DM.

The compensation phase $S(x, y)$ introduced by the deformable mirror can be linearly combined with the response functions of the actuators:

$$S(x, y) = \sum_{i=1}^{97} u_i M_i(x, y) \tag{6}$$

$$M_i(x, y) = exp\{\ln w(\sqrt{(x - x_i)^2 + (y - y_i)^2}/d)^a\} \tag{7}$$

The control signal for the ith actuator is denoted as u, while the influence function of the ith actuator is represented by $M_i(x, y)$. Here, (x, y) refers to the coordinate on the wavefront plane, and (x_i, y_i) represents the coordinate of the ith actuator. The coupling coefficient between actuators—denoted as w—remains constant at a value of 0.1 [32]. Additionally, the Gaussian index with a size of 2 is represented by a, and d denotes the distance between actuators with a size of 2.5 mm.

The mean radius (MR) [33] was employed as the objective function of the optimization algorithm, and it quantified the degree of dispersion of the point spread function (PSF) for the point source imaging. The MR can be expressed as follows:

$$MR = \frac{\iint |(m, n) - (m', n')| I(m, n)\, dm\, dn}{\iint I(m, n)\, dm\, dn}. \tag{8}$$

The coordinate of the image centroid (m', n') is determined through the following calculation:

$$m' = \frac{\iint mI(m, n)\, dm\, dn}{\iint I(m, n)\, dm\, dn}, n' = \frac{\iint nI(m, n)\, dm\, dn}{\iint I(m, n)\, dm\, dn} \tag{9}$$

where $|(m, n) - (m', n')|$ is the distance between the point (m, n) and the image centroid (m', n'). The larger the aberration, the greater the corresponding MR value. The MR gradually decreases as the AO system correction process advances, indicating a reduction in wavefront aberration. We recorded the MR values throughout the iterative process and simultaneously documented changes in the Strehl ratio (SR) for subsequent analysis. The Strehl ratio (SR) is calculated as follows:

$$SR = \frac{Max(I(m, n))}{Max(I_0(m, n))} \tag{10}$$

where $Max(.)$ represents the peak value of the function. $I(m, n)$ is the far-field intensity distribution of distorted wavefronts, and $I_0(m, n)$ is that of the ideal plane wavefront.

3.2. Simulated Results and Analysis

The simulation experiment was realized in the Matlab programming environment. To ensure consistency within the search space, a population size of 50 was set for four algorithms: RUN, PSO, DEA, and GA. Extensive simulations were conducted for each algorithm to select the optimal parameters. In order to evaluate the effectiveness of our proposed AO control method based on the RUN algorithm, a comparative analysis was performed against three other control algorithms (PSO, DEA, and GA), as shown in Figure 4.

The curves that are presented are averaged results obtained from 100 different phase screens when the turbulence level was D/r_0. As illustrated in Figure 4, it is evident that compared to the other three algorithms, the RUN algorithm exhibited significantly faster convergence while achieving optimal values for both the MR and SR.

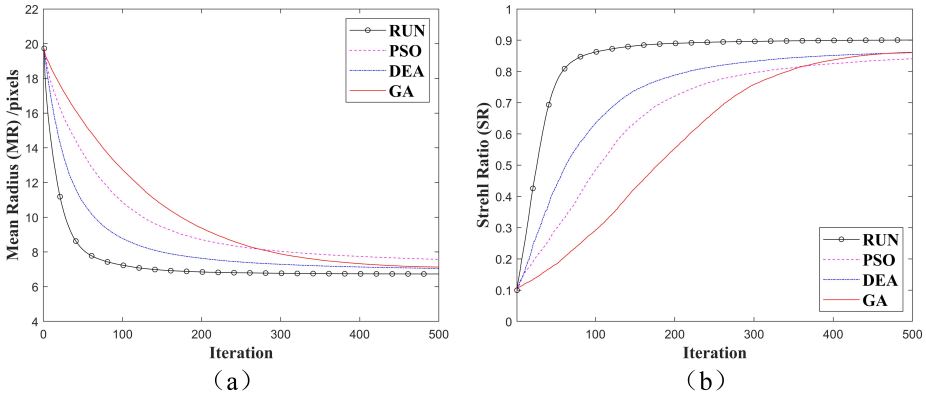


Figure 4. The adaptation process of the adaptive optical system with $D/r_0 = 10$ when using the RUN algorithm, PSO, DEA, and GA as control algorithms. (**a**) MR curves; (**b**) the corresponding SR curves.

Subsequently, we analyzed the convergence speed of the four algorithms. Considering that 80% of the correction range achieved with the RUN optimization algorithm served as the benchmark, we examined the number of iterations required for each algorithm to reach this criterion. The initial averaged MR was 19.72 pixels, while the final MR after applying the RUN optimization algorithm was reduced to 6.73 pixels, which approached the diffraction limit of 4.62 pixels (calculated by using the ideal far-field intensity). This implied that 80% of the MR correction range obtained with the RUN algorithm should have approached a value close to 9.33 pixels. Table 1 presents both the number of iterations needed for different algorithms converging to 9.33 pixels and the final convergence values of the MR. The number of iterations required in Table 1 indicates that the time consumed by the RUN-based control algorithms accounted for 22.6% (1/4.41), 42.5% (1/2.35), and 16.8% (1/5.94) of those of PSO, DEA, and GA, respectively, when achieving equivalent correction performance. The above data show that the AO system based on RUN presented more efficient performance than that of the other three algorithms in terms of convergence speed and correction capabilities.

Table 1. Comparison of the convergence speed and correction results of the RUN algorithm, PSO, DEA, and GA under $D/r_0 = 10$.

	RUN	**PSO**	**DEA**	**GA**
The number of iterations	34	150	80	202
Time consumption (scaled)	1	4.41	2.35	5.94
Final convergence value of the MR	6.73	7.57	7.05	7.13

The correction capabilities of the RUN algorithm were visually evaluated in the comparison of PSFs and wavefronts before and after correction for a random wavefront aberration, as depicted in Figure 5. To facilitate the comparison of changes in the far-field intensity before and after correction, the PSF was normalized according to the ideal intensity distribution, and the light intensity values varied between 0 and 1. It can be clearly seen that the PSF transformed from a diffuse shape before correction into a spot that closely resembled an Airy disk, with a reduction in the MR from 19.71 to 6.51 pixels. Similarly, Figure 5c,d demonstrate effective aberration correction, resulting in a decrease in the root mean square (RMS) from 0.38λ to 0.08λ.

The decomposition of Zernike coefficients ranging from mode 3 to mode 35 before and after correction is illustrated in Figure 6. Based on their magnitudes, it can be inferred that the RUN algorithm effectively corrected these low-mode aberrations.

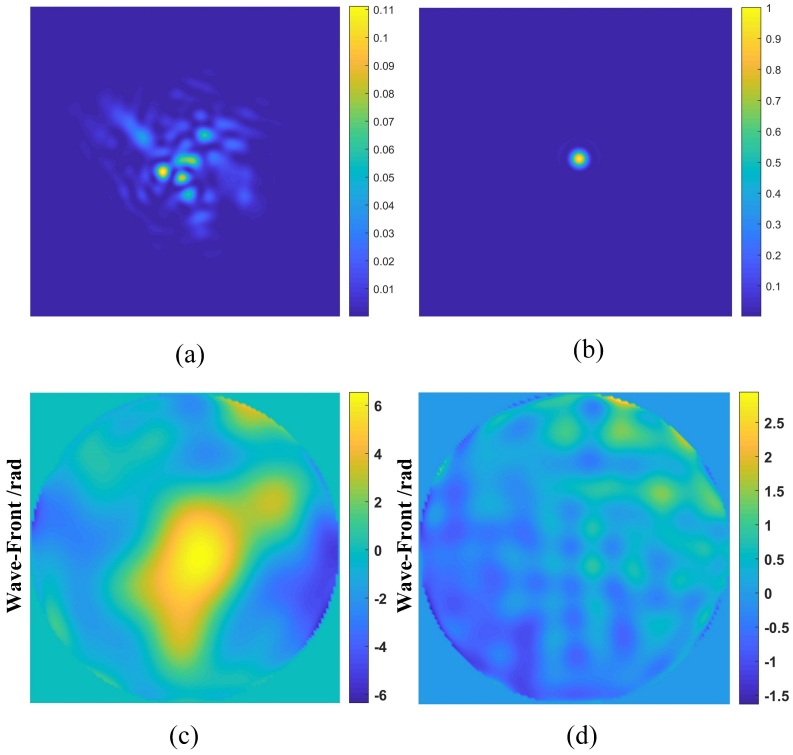


Figure 5. Comparison of PSFs and wavefronts before and after correction: (**a**,**c**) before correction; (**b**,**d**) after correction with the RUN optimizer.

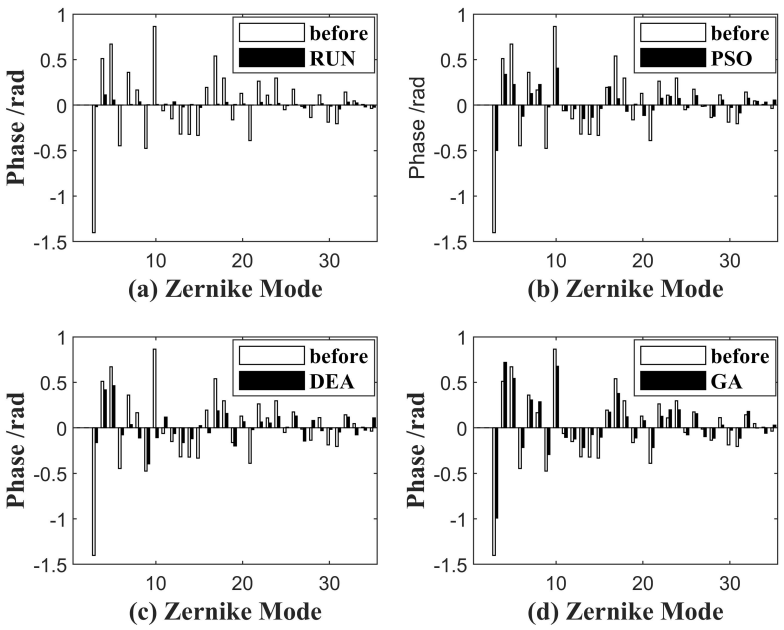
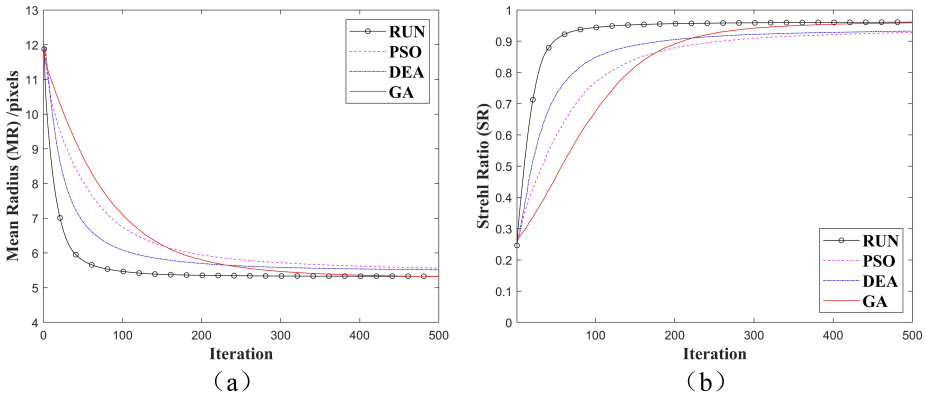


Figure 6. Comparison of Zernike coefficients of modes 3–35 before correction and after correction: (**a**–**d**) RUN, PSO, DEA, and GA, respectively.

In order to thoroughly investigate the adaptation of the adaptive optical system based on the RUN optimizer to different sizes of aberrations, we obtained the following correction results with $D/r_0 = 5$ and $D/r_0 = 25$. Three different turbulence levels ($D/r_0 = 5, 10, 25$) correspond to small, medium, and large wavefront aberrations, respectively.

The curves presented in Figure 7 are the average results obtained from 100 different phase screens when the turbulence level was $D/r_0 = 5$. As shown in Figure 7, it is clear that the RUN algorithm performed best in correcting small aberrations and large aberrations in comparison with the other three algorithms.



(a) (b)

Figure 7. The adaptive process of the adaptive optical system with $D/r_0 = 5$ when using the RUN algorithm, PSO, DEA, and GA as control algorithms. (**a**) MR curves; (**b**) the corresponding SR curves.

Then, we analyzed the convergence speeds of the four different algorithms. Considering that 80% of the correction range achieved with the RUN optimization algorithm served as the benchmark, we examined the number of iterations required for each algorithm to reach this criterion. The initial average MR was 11.87 pixels, and the final MR after applying the RUN optimization algorithm was reduced to 5.33 pixels, which was close to the diffraction limit. This meant that 80% of the MR correction range of the RUN algorithm needed to be close to values around 6.64 pixels. Table 2 shows the number of iterations required for the different algorithms to converge to 6.64 pixels and the final convergence value of the MR. The number of iterations shown in Table 2 shows that the time consumed by the RUN-based control algorithm accounted for 23.6% (1/4.24), 42.4% (1/2.36), and 20.3% (1/4.92) of the time consumed by PSO, DEA, and GA, respectively, when achieving equivalent correction performance. The above data show that the AO system based on RUN presented more efficient performance than that of the other three algorithms in terms of the convergence speed and the correction ability for small aberrations.

Table 2. Comparison of the convergence speed and correction results of the RUN algorithm, PSO, DEA, and GA under $D/r_0 = 5$.

	RUN	**PSO**	**DEA**	**GA**
The number of iterations	25	106	59	123
Time consumption (scaled)	1	4.24	2.36	4.92
Final convergence value of the MR	5.33	5.56	5.51	5.33

The curves presented in Figure 8 are averaged results obtained from 100 different phase screens when the turbulence level was $D/r_0 = 25$. It can be seen in the figure that the RUN algorithm also maintained a good correction effect when correcting large aberrations.

Next, the convergence rates of the four algorithms were analyzed. Using the same criteria, the number of iterations required for each algorithm to achieve this criterion was investigated. After applying the RUN algorithm, the initial average MR was 35 pixels, and the final MR decreased to 12.12 pixels. This meant that the 80% MR correction range of the RUN algorithm needed to be close to 16.7 pixels. Table 3 shows the number of iterations required by the different algorithms to converge to 16.7 pixels and the final convergence value of the MR. As can be seen in Table 3, the number of iterations required by the RUN-based control algorithm to achieve equivalent correction performance accounted for 24.4%

(1/4.10), 55.6% (1/1.80), and 17.1% (1/5.85) of those of PSO, DEA, and GA, respectively. The above data show that the convergence speed and correction ability of the AO system based on RUN were also better than those of the other three algorithms when correcting large aberrations. In the following physical experiments, we investigated the ability of the adaptive optical system based on the RUN optimizer to correct large wavefront aberrations.

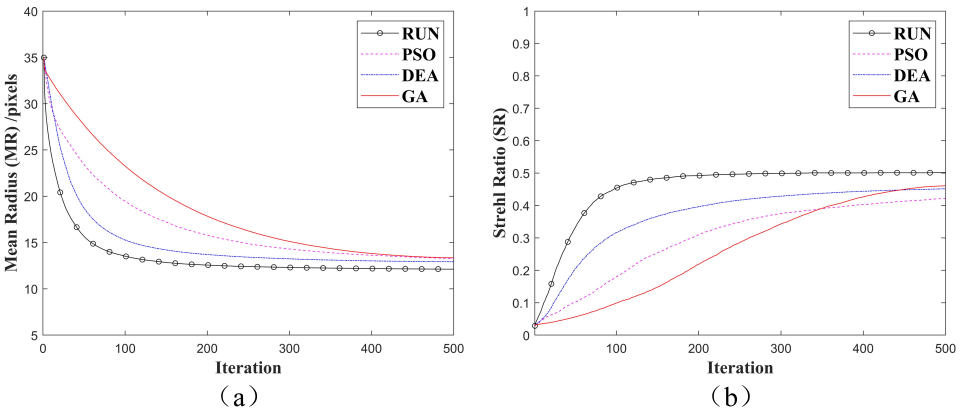


Figure 8. The adaptive process of the adaptive optical system with $D/r_0 = 25$ when using the RUN algorithm, PSO, DEA, and GA as control algorithms. (**a**) MR curves; (**b**) the corresponding SR curves.

Table 3. Comparison of the convergence speed and correction results of the RUN algorithm, PSO, DEA, and GA under $D/r_0 = 25$.

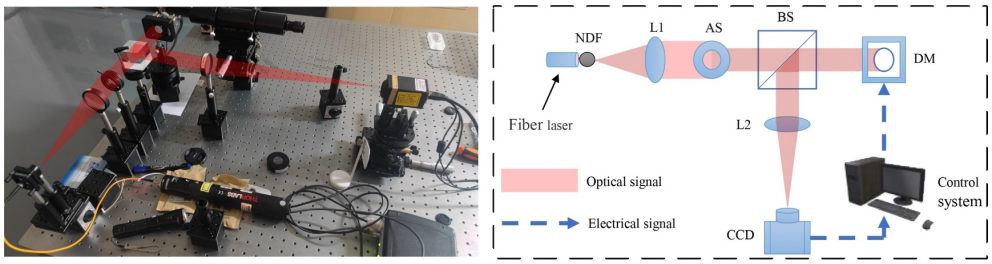
	RUN	**PSO**	**DEA**	**GA**
The number of iterations	40	164	72	234
Time consumption (scaled)	1	4.10	1.80	5.85
Final convergence value of the MR	12.12	13.27	12.92	13.36

4. Physical Experiments and Results for Large Aberrations

4.1. The Experimental System

The experimental setup shown in Figure 9 demonstrated a WFS-less AO configuration based on the RUN optimization algorithm. This system consisted of a laser source operating at a wavelength of 633 nm, a neutral density filter (NDF), an aperture stop (AS) with an effective light-passing aperture of 22.5 mm, a beam splitter (BS), a 97-element DM from the Alpao company with a pitch of 2.5 mm and a diameter of 25 mm, an IMPERX B1020M CCD camera with a pixel size of 5.5 µm, resolution of 1024 × 1024, and depth of 12 bits, lenses L1 and L2 with focal lengths of 200 mm and 400 mm, respectively, and a control system. The programming environment used in the physical experiment was MATLAB2023(a).

The AO system operated in a closed loop, and the RUN optimization algorithm was used to generate driving signals for the deformable mirror. The MR was selected as the metric for the objective function of the control algorithm, with a quasi-static wavefront aberration serving as the object to be corrected. When an incident light wave propagated through the imperfect optical system, it experienced aberrations that led to a distorted input beam. This distorted beam was then reflected by the DM and subsequently imaged onto the CCD camera via lenses. For comparison, we also provide the experimental results when PSO, DEA, and GA were used as control algorithms for the WFS-less AO system.



(a) Experimental device (b) Plane diagram

Figure 9. Experimental WFS-less AO system based on the RUN optimizer.

4.2. The Experimental Results and Analysis

The MR variation curves of the four control algorithms are presented in Figure 10. Upon observing Figure 10, one can see that all four curves converged after 200 iterations, indicating the robust wavefront correction capabilities of these algorithms. However, the MR based on the RUN algorithm exhibited the smallest convergence value, while the MR based on PSO demonstrated the largest convergence value. This signified that the adaptive optical system based on the RUN algorithm possessed higher correction accuracy. Furthermore, the convergence based on the RUN algorithm was also characterized by its swiftness in the convergence curves. Subsequently, a quantitative analysis was conducted to evaluate both the convergence accuracy and speed of each algorithm.

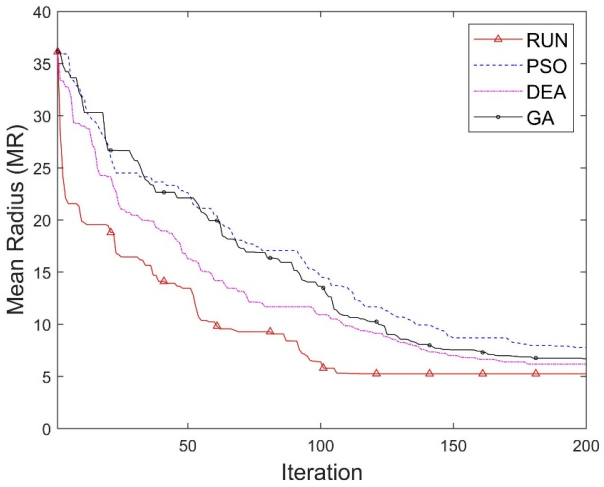


Figure 10. Experimentally obtained curves for the RUN algorithm, PSO, DEA, and GA.

The convergence speed of the RUN optimization algorithm was analyzed by using 80% of its achieved correction range as a benchmark, similarly to the analysis in Section 3.2. The initial MR and final MR were 36.14 and 5.26 pixels, respectively. It was anticipated that the RUN algorithm would reach a value of 11.44 pixels, which corresponded to 80% of its MR correction range. Table 4 presents specific data on the numbers of iterations required by the different algorithms to converge at this target, as well as their final MR convergence values. The RUN algorithm exhibited a faster convergence than that of PSO, DEA, and GA. It required only 54 iterations, while PSO, DEA, and GA needed 124, 98, and 105 iterations, respectively. The convergence speed of the RUN algorithm was approximately 2.30 times faster than that of PSO, and it was 1.81 and 1.94 times faster than those of DEA and GA, respectively.

Table 4. Comparison of the convergence speed and correction results of the RUN algorithm, PSO, DEA, and GA in physical experiments.

	RUN	PSO	DEA	GA
Number of iterations	54	124	98	105
Time consumption (scaled)	1	2.30	1.81	1.94
Final convergence value of the MR	5.26	7.78	6.18	6.70

The diameter of an Airy disk can be calculated using $d = 2.44\lambda f/q$. The resulting diameter d of our experimental system was about 27.46 µm based on the parameters of the experimental system (wavelength: $\lambda = 0.633$ µm, aperture size: $q = 22.5$ mm, and focal length: $f = 400$ mm). The theoretical diameter d, that is, the diffraction limit of this experimental system, was five pixels when the pixel size of the CCD was 5.5 µm. The final MR obtained with the RUN-based AO control algorithm was about 5.26 pixels, which was almost the same as the theoretical diameter of the Airy disk.

The far-field intensity distributions before and after correction using the four algorithms are presented in Figure 11. Figure 11a illustrates the initial far-field intensity, while Figure 11b–e show the corresponding far-field intensity distribution after correction with RUN, PSO, DEA, and GA, respectively. The highest concentration of energy was observed after applying the RUN algorithm. Three-dimensional far-field intensity distributions are shown in Figure 12, where it can be clearly seen that the largest value of central energy was obtained with the RUN algorithm's correction.

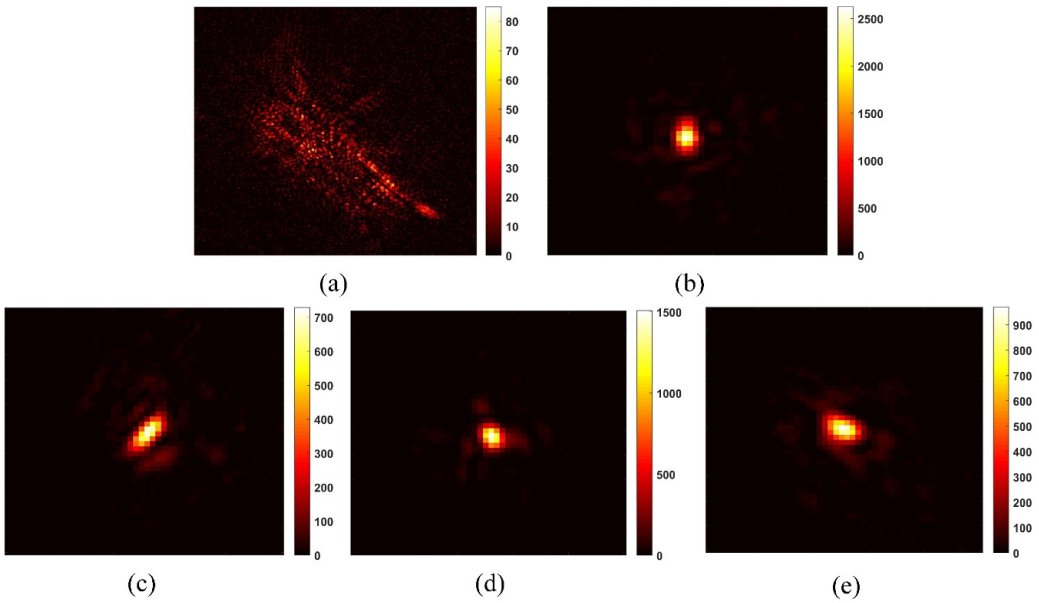


Figure 11. Comparison of far-field intensity distributions: (**a**) before correction; (**b**–**e**) after correction with RUN, PSO, DEA, and GA, respectively.

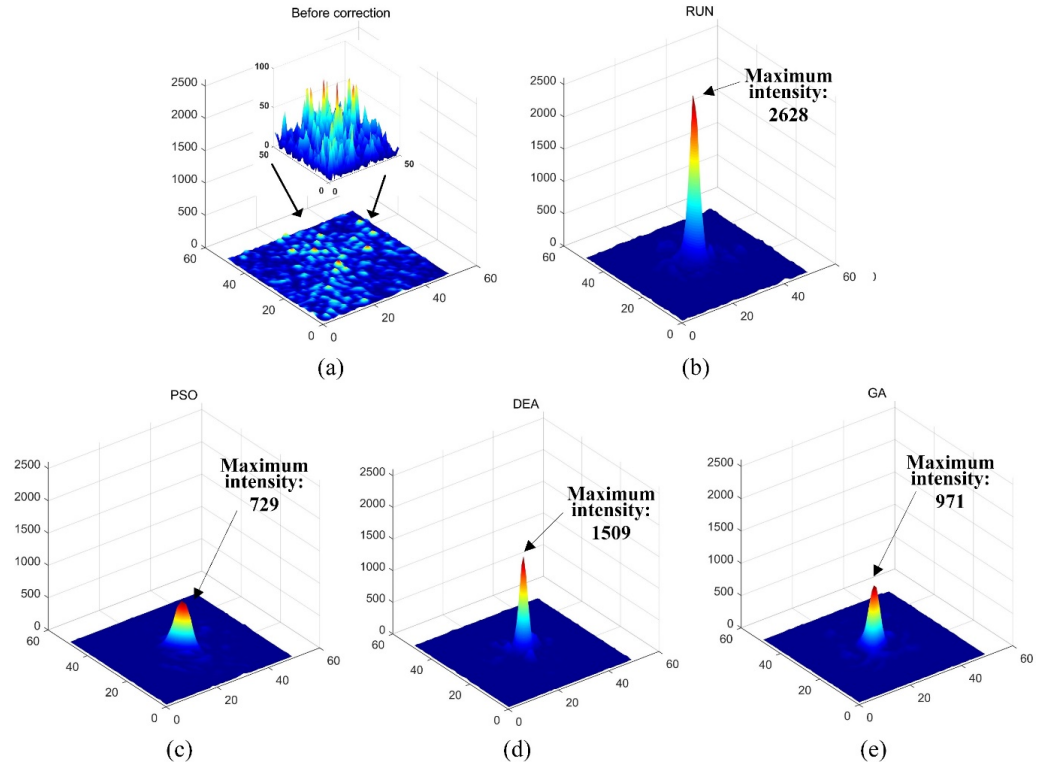


Figure 12. Comparison of 3D far-field intensity distributions: (**a**) before correction; (**b**–**e**) after correction with the RUN algorithm, PSO, DEA, and GA, respectively.

5. Discussion

From Tables 1–3, we can see that the convergence times of the PSO, GA, and DEA control algorithms were about four, five, and two times that of the RUN control algorithm, respectively, regardless of if the aberrations were large or small. However, the convergence times of the PSO, GA, and DEA control algorithms were 2.3, 1.94, and 1.8 times that of the RUN control algorithm, respectively, in the physical experiment. There was a disparity between the convergence speeds in the simulated system and the physical system. This disparity can be attributed to several factors. The noise generated during the CCD acquisition process could have introduced errors in the computation of the performance metrics, thereby potentially impacting the search speed of the metaheuristic algorithms. Additionally, both the simulated and physical experimental results demonstrated similar correction capabilities close to their diffraction limits. It is worth noting that the convergence of the physical system was much closer to its diffraction limit than that of the simulated system. This may have been because the noise of the AO system expanded the search space of the control algorithm to some extent.

The correction of wavefront aberrations in wavefront sensorless (WFS-less) adaptive optical (AO) systems requires control algorithms that can ensure rapid convergence while maintaining effective correction capabilities. In addition, this algorithm is easy to implement and is robust. Generally, different control algorithms for WFS-less AO systems have advantages and disadvantages. RUN is a type of metaheuristic optimization, so we compared several metaheuristic methods for the control of WFS-less AO systems. By synthesizing simulated and experimental data, it was found that the proposed control method was superior to several competing algorithms in terms of its correction speed and correction effect. The correction results at three different turbulence levels showed that the control algorithm based on the RUN optimizer had the fastest convergence speed and the highest convergence accuracy. In addition, the simulations and physical experiments showed that the AO system based on the RUN optimizer was not sensitive to the parameters of the control algorithm, and it was relatively easy to implement. The correction results

for different turbulence conditions also showed the robustness of the AO system based on the RUN optimizer.

Compared with conventional adaptive optics or other WFS-less AO systems, the population algorithm had relatively slow convergence speed, so it is difficult to use it in real-time applications. However, the population algorithm has a strong global search and adaptability, and it can be used in wavefront compensation with low real-time requirements. The control method proposed in this paper was superior to the classical population algorithm in terms of its correction speed and correction effect, and it can be more effectively applied to the fields of light spot shaping, microscope imaging, retina imaging of the human eye, etc.

6. Conclusions

The control algorithm plays a crucial role in determining the correction performance of wavefront sensorless (WFS-less) adaptive optical (AO) systems. We proposed a novel control algorithm based on the RUNge Kutta optimizer for WFS-less AO systems. A simulated AO system and a physical experimental setup with a 97-element deformable mirror were constructed. The convergence speed and correction capabilities of the WFS-less AO system based on the RUN control algorithm were investigated through a simulation analysis and experimental verification. For comparison, we also provided results obtained from the Particle Swarm Optimization (PSO) algorithm, Differential Evolution Algorithm (DEA), and Genetic Algorithm (GA).

The simulated and experimental results consistently demonstrated that our proposed method exhibited a superior correction performance and convergence ratio to those of several competing algorithms. Additionally, the experimental results further validated the effectiveness of our control algorithm in scenarios involving significant aberrations. These research findings can provide a theoretical basis for the practical application of WFS-less AO systems based on the RUN optimization algorithm. The effectiveness of the RUN optimization control method for a point source was verified through simulations and physical experiments in this study. In future research, we will verify the effectiveness of this control algorithm for extended object imaging correction through simulations and physical experiments.

Author Contributions: Conceptualization, H.Y. and Z.Y.; methodology, H.Y. and X.Z.; software, X.Z.; validation, X.Z. and Z.Z.; resources, H.Y. and X.H.; writing—original draft preparation, X.Z.; writing—review and editing, H.Y., P.C. and Y.M.; funding acquisition, H.Y. All authors have read and agreed to the published version of the manuscript.

Funding: National Natural Science Foundation of China (grant no. U2141255, 11873078); the Scientific Research Foundation for High-Level Personnel in Jinling Institute of Technology (jit-rcyj-202301).

Institutional Review Board Statement: Not applicable.

Informed Consent Statement: Not applicable.

Data Availability Statement: The data presented in this study are available on request from the corresponding author.

Conflicts of Interest: The authors declare no conflicts of interest.

References

1. Tyson, R.K. *Principles of Adaptive Optics*, 3rd ed.; CRC Press Inc.: New York, NY, USA, 2010.
2. Muller, R.A.; Buffington, A. Real-time correction of atmospherically degraded telescope images through image sharpening. *J. Opt. Soc. Am. A* **1974**, *64*, 1200–1210. [CrossRef]
3. Vorontsov, M.A.; Carhart, G.W.; Cohen, M.; Cauwenberghs, G. Adaptive optics based on analog parallel stochastic optimization: analysis and experimental demonstration. *J. Opt. Soc. Am. A* **2000**, *17*, 1440–1453. [CrossRef] [PubMed]
4. Pasupathi, T.; Selvi, A.V.J. Real time experimental investigation of adaptive optics compensation technique for free space optical communication. *Photonic Netw. Commun.* **2022**, *44*, 102–115.

5. Stotts, L.B.; Andrews, L.C. Adaptive optics model characterizing turbulence mitigation for free space optical communications link budgets. *Opt. Express* **2021**, *29*, 20307–20321. [CrossRef] [PubMed]
6. Ren, H.; Dong, B. Fast dynamic correction algorithm for model-based wavefront sensorless adaptive optics in extended objects imaging. *Opt. Express* **2021**, *29*, 27951–27960. [CrossRef] [PubMed]
7. Ma, L.; Xu, Q.; Wu, Y.; Yang, H.; Yang, H.; Zhou, Y. Extended Object Imaging Correction for Model-Based Wave front Sensorless Adaptive Optics System Under Noise. *Chin. J. Lasers* **2019**, *46*, 258–264.
8. Poland, S.P.; Wright, A.J.; Girkin, J.M. Evaluation of fitness parameters used in an iterative approach to aberration correction in optical sectioning microscopy. *Appl. Opt.* **2008**, *47*, 731–736. [CrossRef]
9. Yang, W.; Springer, M.; Strohaber, J.; Kolomenski, A.; Schuessler, H.; Kattawar, G.; Sokolov, A. Spectral phase retrieval from interferometric autocorrelation by a combination of graduated optimization and genetic algorithms. *Opt. Express* **2010**, *18*, 15028–15038. [CrossRef]
10. Han, L.; Dai, Y.; Qiu, Y. Compensation for aberrant wavefront in UOWC based on adaptive optics technique employing genetic algorithm. *Optik* **2023**, *281*, 170832. [CrossRef]
11. Yang, H.; Li, Y. Particle Swarm Optimization for Control of Adaptive Optics System. *AISS Adv. Inf. Sci. Serv. Sci.* **2012**, *4*, 390–396.
12. Tehrani, K.F.; Zhang, Y.; Shen, P.; Kner, P. Adaptive optics stochastic optical reconstruction microscopy (AO-STORM) by particle swarm optimization. *Biomed. Opt. Express* **2017**, *8*, 5087–5097. [CrossRef] [PubMed]
13. Hua, Y.; Sui, X.; Zhou, S.; Chen, Q.; Gu, G.; Bai, H.; Li, W. A novel method of global optimisation for wavefront shaping based on the differential evolution algorithm. *Opt. Commun.* **2021**, *481*, 126541. [CrossRef]
14. Chen, B.; Yang, H.; Li, X.; Jiang, W. Adaptive optics correction experiment based on stochastic parallel gradient descent algorithm. In Proceedings of the Fourth International Symposium on Precision Mechanical Measurements, Anhui, China, 25–29 August 2008; SPIE: Bellingham, WA, USA, 2008; Volume 7130, pp. 910–915.
15. Xu, L.; Wang, J.; Yang, L.; Zhang, H. Design and Performance Analysis of NadamSPGD Algorithm for Sensor-Less Adaptive Optics in Coherent FSOC Systems. *Photonics* **2022**, *9*, 77. [CrossRef]
16. Zhang, H.; Xu, L.; Guo, Y.; Cao, J.; Liu, W.; Yang, L. Application of AdamSPGD algorithm to sensor-less adaptive optics in coherent free-space optical communication system. *Opt. Express* **2022**, *30*, 7477–7490. [CrossRef] [PubMed]
17. Zhang, Z.; Luo, Y.; Yang, H.; Su, H.; Liu, J. CoolMomentum-SPGD Algorithm for Wavefront Sensor-Less Adaptive Optics Systems. *Photonics* **2023**, *10*, 102. [CrossRef]
18. Linhai, H.; Rao, C. Wavefront sensorless adaptive optics: A general model-based approach. *Opt. Express* **2011**, *19*, 371–379. [CrossRef]
19. Lianghua, W.; Yang, P.; Shuai, W.; Wenjing, L.; Shanqiu, C.; Xu, B. A high speed model-based approach for wavefront sensorless adaptive optics systems. *Opt. Laser Technol.* **2018**, *99*, 124–132. [CrossRef]
20. Ren, H.; Dong, B. Improved model-based wavefront sensorless adaptive optics for extended objects using N+ 2 images. *Opt. Express* **2020**, *28*, 14414–14427. [CrossRef]
21. Liu, M.; Dong, B. Efficient wavefront sensorless adaptive optics based on large dynamic crosstalk-free holographic modal wavefront sensing. *Opt. Express* **2022**, *30*, 9088–9102. [CrossRef]
22. Hu, K.; Xu, Z.; Yang, W.; Xu, B. Build the structure of wfsless ao system through deep reinforcement learning. *IEEE Photonics Technol. Lett.* **2018**, *30*, 2033–2036. [CrossRef]
23. Landman, R.; Haffert, S.Y.; Radhakrishnan, V.M.; Keller, C.U. Self-optimizing adaptive optics control with reinforcement learning. In Proceedings of the Adaptive Optics Systems VII, Online, 14–18 December 2020; SPIE: Bellingham, WA, USA, 2020; Volume 11448, pp. 842–856.
24. Nousiainen, J.; Rajani, C.; Kasper, M.; Helin, T. Adaptive optics control using model-based reinforcement learning. *Opt. Express* **2021**, *29*, 15327–15344. [CrossRef] [PubMed]
25. Ahmadianfar, I.; Heidari, A.A.; Gandomi, A.H.; Chu, X.; Chen, H. RUN beyond the metaphor: An efficient optimization algorithm based on Runge Kutta method. *Expert Syst. Appl.* **2021**, *181*, 115079. [CrossRef]
26. Kutta, W. Beitrag zur näherungsweisen Integration totaler Differentialgleichungen. *Z. Math. Phys.* **1901**, *46*, 435–453.
27. Runge, C. Über die numerische Auflösung von Differentialgleichungen. *Math. Ann.* **1895**, *46*, 167–178. [CrossRef]
28. Gafar, M.; Ginidi, A.; El-Sehiemy, R.; Sarhan, S. Improved SNS algorithm with high exploitative strategy for dynamic combined heat and power dispatch in co-generation systems. *Energy Rep.* **2022**, *8*, 8857–8873. [CrossRef]
29. Chen, H.; Ahmadianfar, I.; Liang, G.; Bakhsizadeh, H.; Azad, B.; Chu, X. A successful candidate strategy with Runge-Kutta optimization for multi-hydropower reservoir optimization. *Expert Syst. Appl.* **2022**, *209*, 118383. [CrossRef]
30. Roddier, N.A. Atmospheric wavefront simulation using Zernike polynomials. *Opt. Eng.* **1990**, *29*, 1174–1180. [CrossRef]
31. Hardy, J.W. Adaptive optics for astronomical telescopes. *Phys. Today* **1998**, *53*, 69–69. [CrossRef]

32. Jiang, W.; Ling, N.; Rao, X.; Shi, F. Fitting capability of deformable mirror. In Proceedings of the Active and Adaptive Optical Systems, San Diego, CA, USA, 21–21 July 1991; SPIE: Bellingham, WA, USA, 1991; Volume 1542, pp. 130–137.
33. Piatrou, P.; Roggemann, M. Beaconless stochastic parallel gradient descent laser beam control: numerical experiments. *Appl. Opt.* **2007**, *46*, 6831–6842. [CrossRef]

Disclaimer/Publisher's Note: The statements, opinions and data contained in all publications are solely those of the individual author(s) and contributor(s) and not of MDPI and/or the editor(s). MDPI and/or the editor(s) disclaim responsibility for any injury to people or property resulting from any ideas, methods, instructions or products referred to in the content.